# Comparison between two profile migration methods

*Kamal Al-Yahya*


## ABSTRACT

Profile migration require downward continuing both source and receivers. Instead of downward continuing the source and cross-correlating it with the downward-continued receivers, I use ray tracing to time-shift the downward-continued receivers. The differences between the two methods are minor, the most important one being a phase shift of $\pi/4$.


## INTRODUCTION

It is possible to do profile migration by downward continuation of the surface wave field followed by time shifting. The amount of the time shift for a receiver is equal to the travel time from the source to that receiver at the new depth (after extrapolation). The image at $t = 0$ is then mapped to the output at that depth. This method therefore mixes wave-theoretical extrapolation with ray-theoretical time shifting. This (hybrid) scheme, discussed in Al-Yahya (1984), is shown in Figure 1. Within the domain of ray theory, this method is equivalent to downward continuing both the source and receivers and applying an appropriate imaging principle (discussed below). In this paper, I will show the differences and similarities between these two methods.

## THE TWO METHODS

The reflectivity of the subsurface, $R$, can be defined as the ratio of the upgoing field to the downgoing field (Clærbout, 1985). For a given frequency, $\omega$,

$$\begin{aligned} R(x,z,\omega) &= \frac{U(x,z,\omega)}{D(x,z,\omega)} \\ &= \frac{U(x,z,\omega)D^*(x,z,\omega)}{D(x,z,\omega)D^*(x,z,\omega)} \\ &= \frac{U(x,z,\omega)D^*(x,z,\omega)}{|D(x,z,\omega)|^2} , \end{aligned} \tag{1}$$

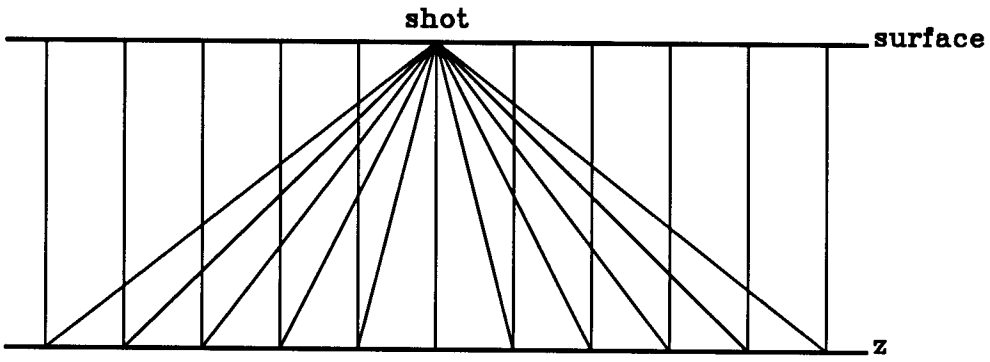


FIG. 1. A schematics diagram of profile migration by the hybrid method. Vertical lines are the downward continuation paths and slanted lines are the time shifting paths.

where * denotes conjugation. $UD^*$ is the cross-correlation between the upgoing and downgoing fields in the frequency domain and integration over $\omega$ gives the zero-lag cross-correlation. At any given frequency, the denominator in (1) is a divergence correction that depends on $x$ and $z$. Because of the instability of dividing by $|D|^2$, some people ignore this factor. Others add a damping constant in the denominator (which I have found to be unsatisfactory).

The extrapolation can be done using either finite differencing or phase shifting; the latter will be used here. The downgoing field will be that of a line source because in the frequency-wavenumber domain, we have $k_y = 0$ which is equivalent to integrating along the $y$-axis; integrating point sources along the $y$-axis turns them into line sources. The Green's function for a line source is

$$G(k_x, z, \omega) = \frac{e^{-ik_z z}}{ik_z} \ .$$

The division by $k_z$ is equivalent to applying a cosine correction. This correction is needed because we have a line source that causes an amplitude variation with offset at a given depth. It is ignored in zero-offset migration because each receiver is assumed to be associated with a source directly below it (in the exploding-reflector model).

To obtain the migrated image, we first extrapolate the field recorded at the surface, $p(x, z = 0, t)$, to the depth $z$ by applying a phase shift in the frequency-wavenumber domain (just like is done in post-stack migration),

$$p(k_x, z, \omega) = p(k_x, 0, \omega) e^{-iz\sqrt{\frac{\omega^2}{v^2} - k_x^2}} \ . \tag{2}$$

In equation (2), a constant velocity is assumed. For convenience, this assumption will be held in the rest of the discussion, although the arguments can be extended to the non-constant velocity case. By the same argument used for the source, equation (3) also assumes line receivers.

Since both imaging methods have to be done in the space domain, we need to Fourier

transform equation (2),

$$p(x,z,\omega) = \int p(k_x,0,\omega) e^{-iz\sqrt{\frac{\omega^2}{v^2}-k_x^2}} e^{-ik_x x} dk_x \ . \tag{3}$$

We can now do the same thing to the source and then apply the imaging principle in (1) to get the reflectivity at a given frequency. The migrated image (at $t = 0$) is obtain by adding all frequencies,

$$p_1(x,z,t=0) = \int \left[ \int p(k_x,0,\omega) e^{-iz\sqrt{\frac{\omega^2}{v^2}-k_x^2}} e^{-ik_x x} dk_x \right] \left[ \int \frac{e^{-iz\sqrt{\frac{\omega^2}{v^2}-k_x^2}}}{i\sqrt{\frac{\omega^2}{v^2}-k_x^2}} e^{-ik_x x} dk_x \right]^* |D(x,z,\omega)|^{-2} \, d\omega \ . \tag{4}$$

Instead of the imaging principle (1), we can use an imaging principle that is similar to the one used in post-stack migration. In post-stack migration, with the exploding reflector model, the image is taken to be at $t = 0$ after extrapolation. In profile migration, the image is taken to be at $t = \tau$ where $\tau$ is the travel time from the source to the receiver at that depth. Alternatively, we can shift the extrapolated field by $\tau$ and take the image at $t = 0$. For a constant-velocity model, $\tau = \sqrt{x^2+z^2}/v$ and the migrated gather is

$$\begin{aligned} p_2(x,z,t=0) &= \int \left[ \int p(k_x,0,\omega) e^{-iz\sqrt{\frac{\omega^2}{v^2}-k_x^2}} e^{-ik_x x} dk_x \right] e^{+i\frac{\omega}{v}\sqrt{x^2+z^2}} \sqrt{x^2+z^2} \, d\omega \\ &= \int \left[ \int p(k_x,0,\omega) e^{-iz\sqrt{\frac{\omega^2}{v^2}-k_x^2}} e^{-ik_x x} dk_x \right] \left[ \frac{e^{-i\frac{\omega}{v}\sqrt{x^2+z^2}}}{\sqrt{x^2+z^2}} \right]^{-1} d\omega \end{aligned} \tag{5}$$

where a divergence correction is also applied by multiplying by $\sqrt{x^2+z^2}$.

Note that in both (4) and (5), the extrapolation of receivers is done in the same way. The difference between the two equations is in the source-extrapolation terms.

## GREEN'S FUNCTIONS

The last term in the integrand of (5) is nothing but the reciprocal of the Green's function of a point source. Figure 2 compares it to the conjugate of the Green's function of a line source in (4) for a given depth and frequency. The figure shows that there is both an amplitude and a phase difference between the two functions.

To explain the differences that appear in Figure 2, let's compare the two Green's functions in the space domain. The Green's function for a line source is the Hankel function of zero order. This is easily obtained by noting that the general solution of the wave equation in cylindrical coordinates is a linear combination of the zero-order Hankel functions of the first and second kind,

$$G(r,\omega) = c_1 H_0^{(1)}(\frac{\omega}{v} r) + c_2 H_0^{(2)}(\frac{\omega}{v} r) \ ,$$

where $c_1$ and $c_2$ are constants (for a given frequency) and $H_0^{(1)}(.)$ represents the outward traveling wave while $H_0^{(2)}(.)$ represents the inward traveling wave. If we have a line source,

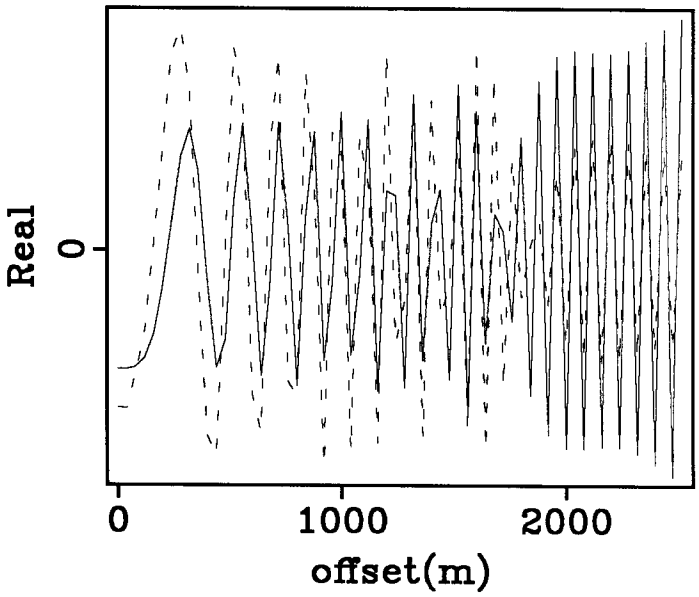


FIG. 2. (a) The real part of the source-extrapolation terms at a given depth and frequency. The solid line is for a point source and the dashed line is for a line source. Parameters for this and the next figure are: frequency=45 Hz, $v$=3 km/sec, $dx$=40 m, $z$=1.5 km. Both functions have been normalized to get rid of multiplicative constants.

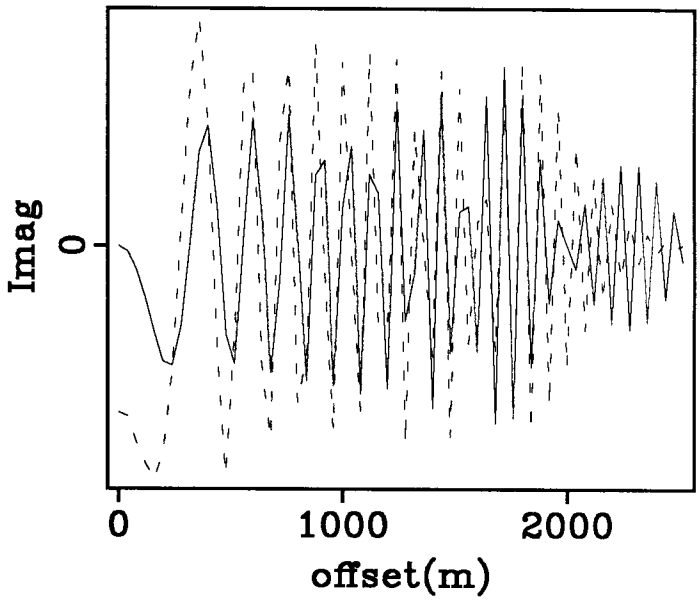


FIG. 2. (b) The imaginary part of the source-extrapolation terms at a given depth and frequency. The solid line is for a point source and the dashed line is for a line source.

then there is only an outward traveling wave and therefore

$$G(x,z,\omega) = c_1 \, H_0^{(1)}(\frac{\omega}{v}\sqrt{x^2+z^2}) \; . \tag{6}$$

For large arguments, the Hankel function has the asymptotic expansion

$$H_0^{(1)}(a) \approx \sqrt{\frac{2}{\pi a}} \, e^{-i(a-\frac{\pi}{4})} \; ,$$

Abramowitz and Stegun (1965) (for small arguments it has a logarithmic singularity). Therefore, for large arguments, the Green's function for a line source is,

$$G(x,z,\omega) \sim \sqrt{\frac{v}{\omega\sqrt{x^2+z^2}}} \, e^{-i(\frac{\omega}{v}\sqrt{x^2+z^2}-\frac{\pi}{4})} \; , \tag{7}$$

which I will take to represent $D$ in (4). The large argument requirement in (7) means it is valid for the far field or high frequency, namely when ray theory applies.

## DISCUSSION

The first difference between (4) and (5) is the $\pi/4$ phase shift that is found in (7). This phase shift is clearly observed in Figure 2 and the amount of phase shift is verified by applying a $\pi/4$ phase shift to the dashed line as shown in Figure 3.

The second difference between (4) and (5) is the divergence correction. In (5), the divergence correction is $\sqrt{x^2+z^2}$. To obtain the divergence correction in (4), we need to compute $|D|^{-2}$. From (7),

$$\begin{aligned} |D(x,z,\omega)|^{-2} &\sim \omega \, (x^2+z^2)^{\frac{1}{2}} \\ &= \omega \, div(x,z) \; , \end{aligned} \tag{8}$$

where $div(x,z)$ is a divergence correction (note that it is the same as the divergence correction in (5)). Adding this divergence correction, we see in Figure 4 that the amplitudes become much similar. It is important however to note that the figures shown are for *one* frequency. When adding the various frequency components using equation (4), these weights are $\omega$-dependent. These weights come from two places. The first is $\omega$ in (8) and the second is the coefficient $a$ in (6) (remember it is $\omega$-dependent).

The differences between the two methods are not expected to produces big differences in the final migration result. In comparing the two methods in migrating a synthetic profile, I ignored the denominator $|D|^2$ in (1) (for stability reasons). Figure 5 shows that the two methods gave the same image except for a difference in the amplitude. The images at a given depth from both parts of Figure 5 are compared in Figure 6a which shows the predicted phase shift. The amount of the phase shift is verified in Figure 6b to be $\pi/4$ by applying a $\pi/4$ phase shift to the dashed line.

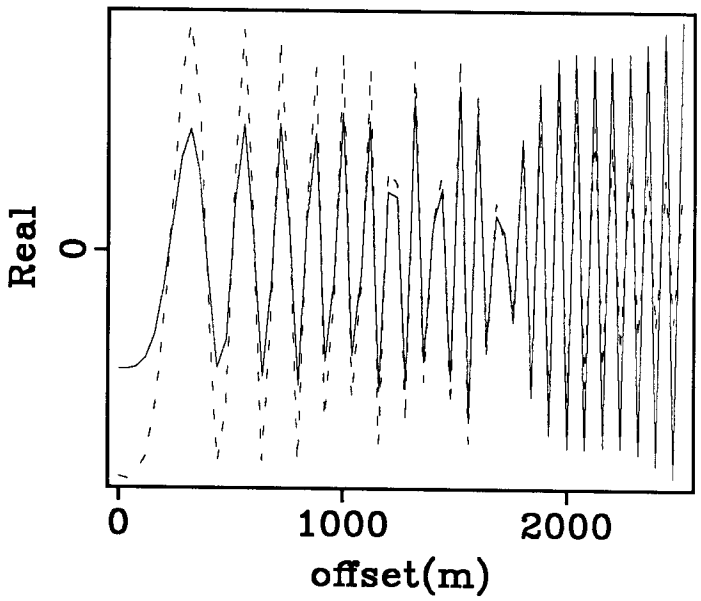


FIG. 3. (a) The result of applying a phase shift of $\pi/4$ to the dashed line of Figure 2(a)

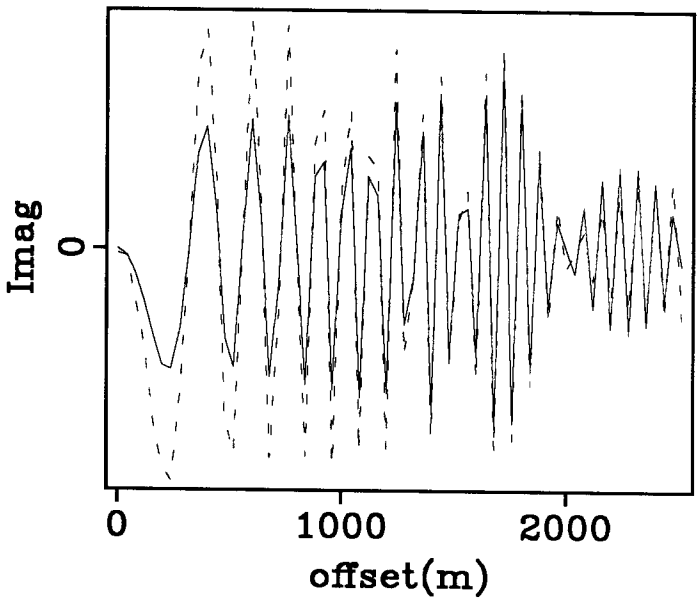


FIG. 3. (b) The result of applying a phase shift of $\pi/4$ to the dashed line of Figure 2(b)

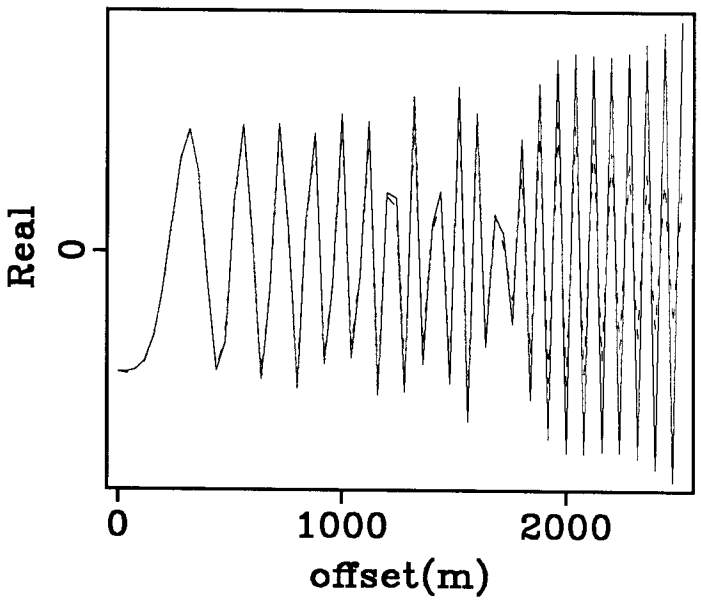


FIG. 4. (a) The result of changing the divergence correction of the dashed line in Figure 3(a). The functions were scaled so that they match at small offsets

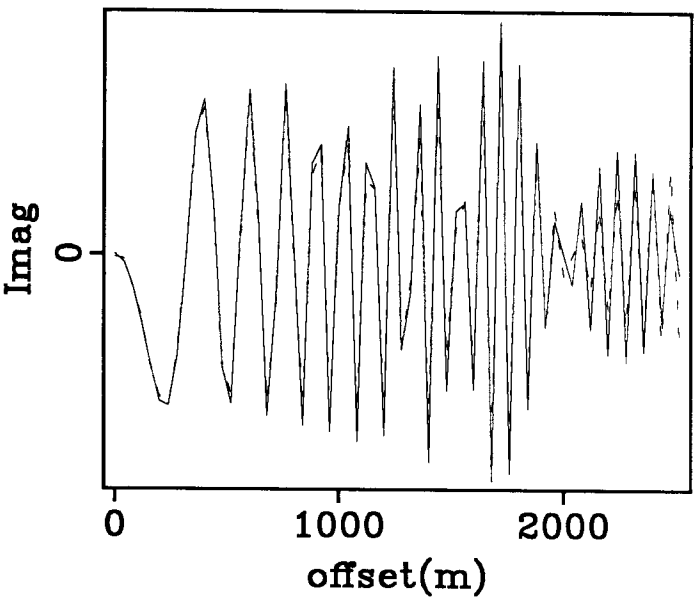


FIG. 4. (b) The result of changing the divergence correction of the dashed line in Figure 3(b). The functions were scaled so that they match at small offsets

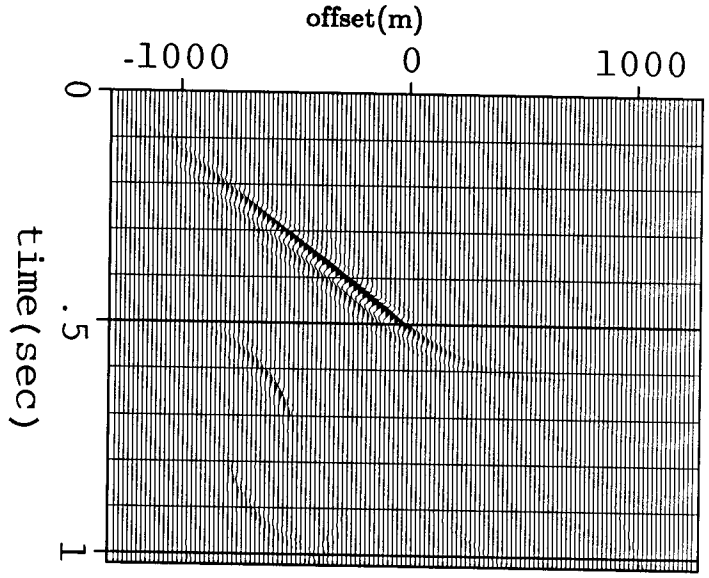


FIG. 5. (a) A dipping reflector migrated by downward continuation of both source and receivers and cross-correlating.

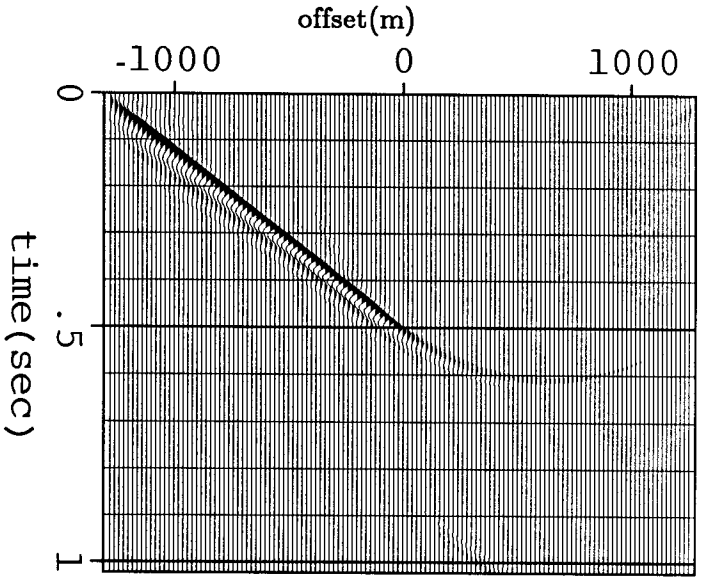


FIG. 5. (b) A dipping reflector migrated by downward continuation of receivers and then time-shifting.

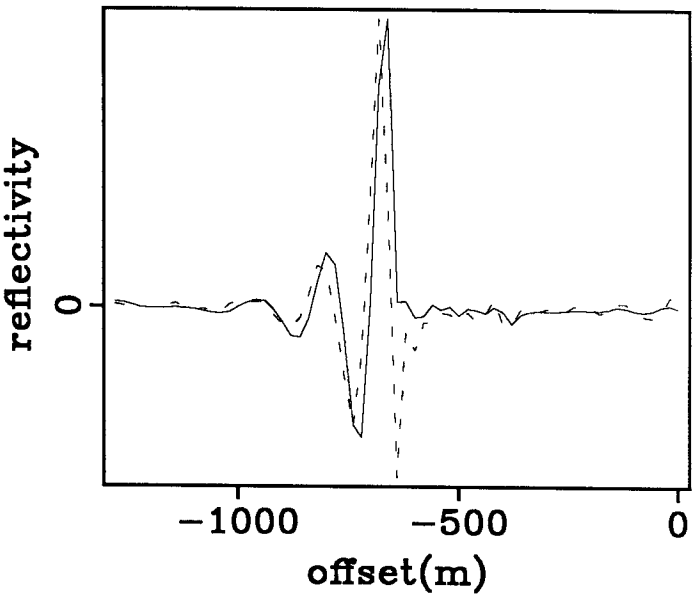


FIG. 6. (a) Images at travel-time depth=.25 sec taken from Figure 5. The solid curve is from Figure 5a and the dashed curve is from Figure 5b. Note the phase shift between the two curves.

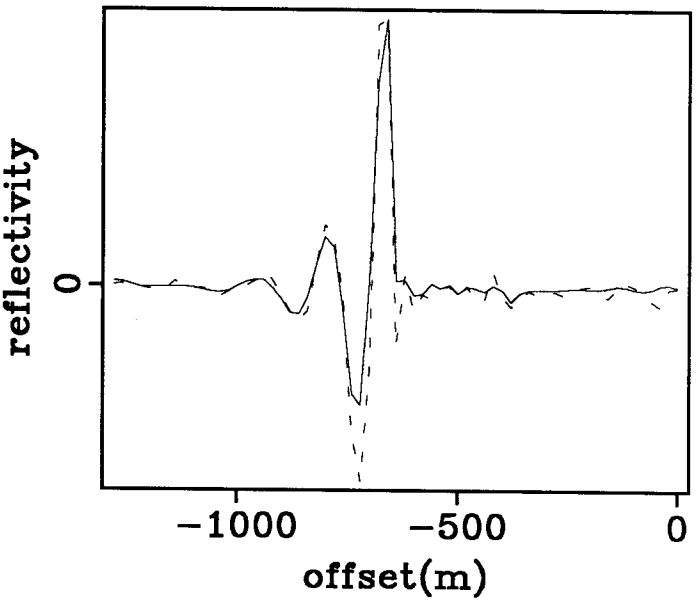


FIG. 6. (b) The result of applying a $\pi/4$ phase shift to dashed line in Figure 6a.

## CONCLUSIONS

When ray theory applies, profile migration by extrapolation and time shifting is equivalent to downward continuation of both source and receivers and cross-correlation. The main differences between the two methods is the divergence correction and a phase-shift of $\pi/4$.

## ACKNOWLEDGMENTS

I would like to thank Francis Muir who suggested this study and gave useful suggestions. Thanks also to Pete Mora and Jos van Trier for reviewing the paper and giving valuable suggestions.

## REFERENCES

Abramowitz, M. and Stegun, I.A., 1965, Handbook of mathematical functions, Dover Publications, New York, p. 364.

Al-Yahya, K., 1984, Velocity analysis using prestack migration, SEP–38, p. 105-112.

Clærbout, J.F., 1985, Imaging the earth's interior, Blackwell Scientific Publication, p. 376-378.